INSTITUTE OF PHYSICS PUBLISHING METROLOGIA
Metrologia **40** (2003) S78–S80 PII: S0026-1394(03)57718-0

Calibration of the total irradiance monitor

G M Lawrence, G Kopp, G Rottman, J Harder, T Woods and H Loui

Laboratory for Atmospheric and Space Physics, University of Colorado, Boulder, CO 80309-0590, USA

E-mail: George.Lawrence@lasp.colorado.edu

Published 7 February 2003
Online at stacks.iop.org/Met/40/S78

Abstract
Launching on the SORCE (SOlar Radiation and Climate Experiment), the total irradiance monitor (TIM) will measure the total solar irradiance to a relative standard uncertainty of 10^{-4} and a noise level of 2×10^{-6} each 400 s. Because of the outstanding brightness, uniformity, stability and collimation of the Sun, this ambient temperature primary radiometer achieves an absolute accuracy comparable to that of a cryogenic radiometer. The major paradigm shift from previous solar radiometers is the use of phase-sensitive detection at the shutter fundamental. We describe the equivalence between replacement power and radiant power as a complex number, the ratio of the (complex) thermal impedances. Our aperture measurements are provided by NIST, with added corrections for diffraction and scattering. We measure the cavity reflection losses versus wavelength using laser scans. We have verified methods for measuring, in flight, the servo gain, cavity reflection changes and shutter-modulated infrared offset (dark signal).

1. Total irradiance monitor

The total irradiance monitor (TIM) is an ambient temperature, electrical substitution, null-balance, solar radiometer [1, 2] and was launched in January 2003 on NASA's SOlar Radiation and Climate Experiment (SORCE) satellite to measure the total solar irradiance (TSI). The instrument is ready for flight and we argue here that we will achieve 10^{-4} relative standard uncertainty in TSI. To better understand the thermal circuits and to provide precision near 10^{-6}, we apply phase-sensitive detection [3] at the shutter fundamental frequency (10 mHz, 100 s period). This detection method reduces sensitivity to thermal drifts, $1/f$ noise and parasitic thermal emission from the heat sink (which will be out-of-phase with the shutter). Similar techniques are planned for the upcoming NISTAR radiometer and used in an ambient temperature prototype [4].

The measurement equations (1) and (2) for the TIM follow from the path of 'signals' indicated in figure 1. Signals are complex Fourier components (bold type) representing the amplitude and phase of sinusoidal variations [5, 6] versus frequency. These complex numbers describe shutter transmission, power, temperature, voltage and data numbers at various places within the TIM. We analyse the TIM signals at frequencies between 0 Hz and 50 Hz, but determine the irradiance at the shutter fundamental. The data numbers D in figure 1 emerge at a clock rate up to 100 s^{-1}, providing 10^4 numbers per shutter cycle. In ground processing, the time series D is Fourier analysed and smoothed, then corrected for dark signal and gain to produce an in-phase data number component $\tilde{D}$ defined in (2). The TSI E_0 is then determined from

$$E_0 = \frac{V^2}{\alpha A R f} \frac{\tilde{D}}{M} \tag{1}$$

where A is the aperture area and α is the absorptance of the cavity. The flight standard voltage V and the standard resistor R provide the standard watt, V^2/R. An average fraction $\tilde{D}/M$ of this power, with $M = 64\,000$, is applied to the active cavity by a digital pulse width modulator. Four factors are combined in f to correct Doppler changes, distance to the Sun, degradation and pointing effects. All parameters in (1) are real.

Feedforward data numbers F are applied at shutter openings to anticipate the servo system response to incident radiation changes. The corrected fundamental component of

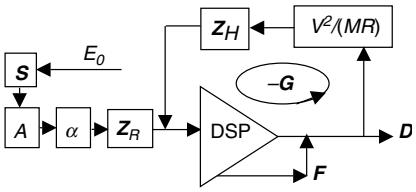

Figure 1. Signal transfer diagram from irradiance E_0 in to data numbers D out. Variables in boxes are out/in ratios at some frequency. The servo loop gain is $-\boldsymbol{G}$. The digital signal processor (DSP) adds a known feedforward signal $\boldsymbol{F}$. The ratio of thermal impedances $\boldsymbol{Z}_H/\boldsymbol{Z}_R$ is the equivalence ratio.

the data numbers, $\tilde{D}$, is obtained from

$$\tilde{D} = \text{real}\left\{\frac{-(\mathbf{Z}_H/\mathbf{Z}_R)\text{FT}(D_J + ((D-F)_J/G))}{\text{FT}(S)}\right\} \quad (2)$$

where FT() is the Fourier transform, D are the data numbers, S is the shutter waveform and $\mathbf{Z}_H/\mathbf{Z}_R$ is the equivalence ratio. Measurements of empty space during the eclipse portion of each orbit along with temperature monitors in TIM provide a similar $\tilde{D}_{\text{dark}}$ of the instrument's thermal ('dark') signal during the solar measurement. We set F close to D to make the gain-dependent term small. The corrected data numbers are smoothed with four boxcar averages, each 100 s wide. The smoothing filter has a total width of 400 s and a standard deviation of 57.7 s. The TSI is computed every 100 s.

2. Relative standard uncertainties

Table 1 summarizes our analyses of the relative standard uncertainty, u. These estimates, described in section 3, are assembled from NIST calibrations, analyses, repeatability and Monte Carlo calculations based on parameter uncertainties. The dominant uncertainties are in the aperture A and the cavity absorption α.

3. Component calibrations

The areas A of the diamond-turned aluminium apertures were measured ($u = 25 \times 10^{-6}$) at NIST [7], and are corrected for temperature changes and diffraction. Eric Shirley of NIST [8, 9] advises that we include 10% (4.5×10^{-5}) of the diffraction correction as uncertainty. We include, based on measurements, uncertainties due to scattering effects from imperfect edges. The diffraction correction is proportional to the wavelength, so the solar diffraction correction is proportional to the energy-weighted average wavelength $\bar{\lambda}$ of the solar spectrum. Measured solar spectra [10] give $\bar{\lambda} = 947$ nm.

We measured cavity reflectance $1 - \alpha$ using laser scans of the cavity interiors, averaging the map over the central illumination region. Seven laser wavelengths (457 nm, 532 nm, 633 nm, 830 nm, 1064 nm, 1523 nm, and 10 600 nm) span the solar spectrum, with the effective cavity reflectance being the solar-weighted average of the measurements (see figure 2). Measurements using NIST's FTIR [11] indicate that the infrared reflectances are smooth and continuous with wavelength. The interpolation between the discrete wavelengths is a spline fit of the reflectance versus wavelength. This fit is constrained at long wavelengths by estimating a reflectance at 100 μm that maintains a smoothly decreasing slope so the fitted long-wavelength reflectance never exceeds unity. The effective solar-weighted reflectances for the four TIM cavities are (169, 139, 307, 360) $\times 10^{-6}$. Reflectance uncertainties are ≈10% Type B and ≈10% Type A for an rss (root-sum-square) total of 14%.

Over three years of operation, five laboratory copies of the standard voltage circuits have changed in relative voltage by $-(1 \pm 1) \times 10^{-6}$ year^{-1}, consistent with previous studies [12]. We will correct at this rate and continue to watch these five, plus four more units. The flight standard voltages have been stable to $<10^{-6}$ in spite of six qualification temperature cycles from −35 °C to +50 °C. The voltage temperature coefficients of the two flight standard voltages are -1×10^{-7}/°C and -2×10^{-7}/°C.

The standard resistors are wound on the back of the cavities, epoxy encapsulated, then plated with copper and gold. The measured temperature coefficients of resistance range from 8×10^{-6}/°C to 10×10^{-6}/°C, close to the specification of the heater wire. The temperature cycling has changed their relative resistance by less than 3×10^{-6}. The copper lead resistances are corrected against four different instrument temperatures. Both the standard voltage and the standard resistors have been repeatedly measured to track consistency up to launch.

The shutter moves between a transmission of 1 when open and a transmission $<3 \times 10^{-6}$ when closed. The operation delay and transition times are about 10 ms. Given the 100 s shutter period, these parasitic times produce a relative correction $<10^{-6}$ in the Fourier transforms of (2).

The field-of-view map shows $<10^{-4}$ relative response past 10° off-axis. This rejection suffices to restrict contamination by Earthshine to <2.5 min at orbital sunrise and sunset.

Noise measurements with the completed instrument give noise levels of $<2 \times 10^{-6}$ at the shutter fundamental. We minimize the noise by placing the shutter fundamental near

Table 1. Summary of uncertainty u.

Factors/corrections	Size $\times 10^6$	$u \times 10^6$
Ephemeris f	35000	3
Shutter $\boldsymbol{S}$		3
Aperture A		25
A correct	454	52
Reflectance $1 - \alpha$	168–360	24–51
Servo gain $\boldsymbol{G}$	100	0.1
Standard V^2		10
Standard R		10
R correct	121	5
Equivalence $\mathbf{Z}_H/\mathbf{Z}_R$		20
Dark signal	2700	1
Root-sum-square (rss) total		66–80

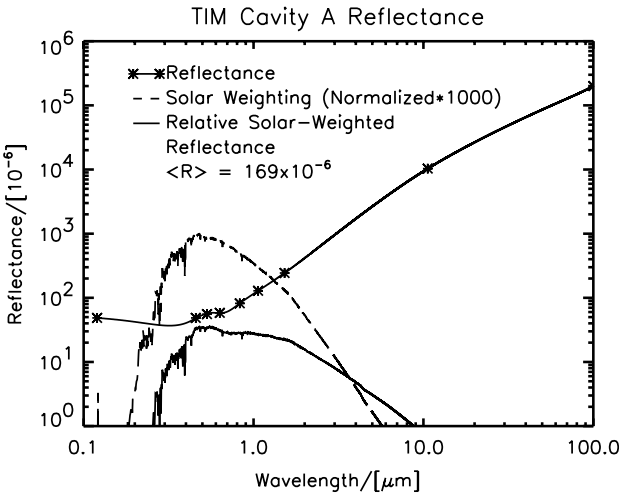

Figure 2. The measured reflectance for the TIM cavity (∗) increases with wavelength. The cavity reflectance is weighted by the relative solar spectral irradiance (- - - -), giving a relative solar-weighted cavity reflectance (——).

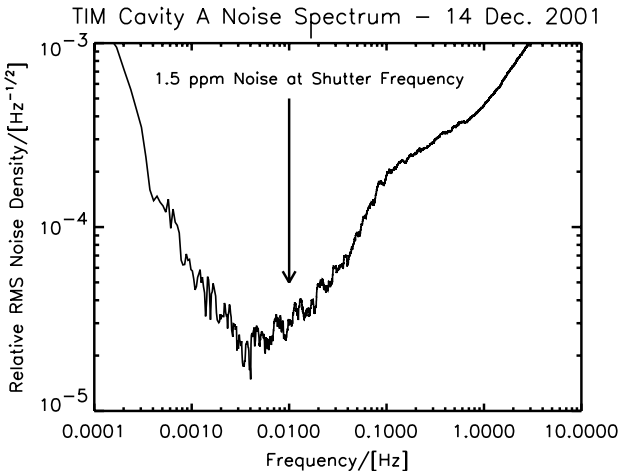

Figure 3. The measured noise power density gives $<2 \times 10^{-6}$ relative noise at the shutter frequency, given the TIM filter root-bandwidth of 0.05 $Hz^{1/2}$.

the minimum of the noise spectrum (figure 3). The remaining noise is intrinsic to the thermistors on the cavities.

Because of calibration measurement uncertainties, there will be differences between the four cavities in measured TSI. The differences will be adjusted using a weighted average based on the uncertainty of measurement accuracy with each cavity.

4. In-flight calibrations

We approximate the dark signal by observing space during the dark sides of each orbit, fitting the transformed data numbers (2) to instrument temperatures, then interpolating to the Sun side. Models indicate this dark signal will be $\approx 3 \times 10^{-3}$ of the solar irradiance, with relative changes of $\approx 10^{-4}$ between orbital sunset and sunrise. Temperature readings from the cavities, the front and rear of the heat sink, the pre-baffle and the shutters form the basis vectors for fitting the observed dark signals as a linear combination:

$$\tilde{D}_{\text{dark}} \approx \sum_{J=1}^{5} C_J T_J^4 \qquad (3)$$

where the C_J are determined for best fit and T_J are the temperatures in kelvin. Since the temperatures all rise or fall together, and vary by a small fraction of their average, the basis vectors in (3) are highly correlated. To isolate the significant variation in data numbers, we use the singular value decomposition (SVD) method [13]. The coefficients in (3) will be ill-determined, but the model will give accurate predictions of the IR background signal. The calculations indicate that the interpolation will have an uncertainty of $<5 \times 10^{-6}$ for data from *only one orbit*. Continued application of the algorithm will reduce the uncertainty in dark signal to $<10^{-6}$.

To track degradation due to solar exposure, we will make measurements with cavity A all the time, cavity B 1% of the time, cavity C 0.1% of the time and cavity D annually. Any exposure effects can thus be tracked and corrected by a degradation factor that starts at 1 at launch. A ground program to monitor unused witness cavities will determine reflectance changes due to aging. To differentiate between cavity absorptance changes and other system changes, the baffles contain small silicon photodiodes, monitoring the reflection from each cavity. Their resolution will be better than 0.1% of the reflection; so given a reflectance of 5×10^{-4}, the resolution on relative changes in absorptance is $<5 \times 10^{-7}$.

The servo gain is calibrated by the DSP monthly to an accuracy of 10^{-5}. We further set the feedforward (2) $F \approx D$ within 1% with the real part of $1/G \approx 1/60$. Therefore, the gain-dependent term in (2) is a relative correction of $\sim 10^{-4}$ with relative uncertainty $<10^{-7}$.

The equivalence ratio $\boldsymbol{Z}_H/\boldsymbol{Z}_R$ in (2) and figure 1 comes largely from model calculations and is very near unity with an uncertainty of $<2 \times 10^{-5}$ [1]. This uncertainty occurs only at the shutter fundamental frequency. The non-equivalence at the higher harmonics is larger, however, and will be used to further constrain the equivalence models. Essentially, the responses at the third and fifth harmonics determine the thermal delay and attenuation of the cavities using the Sun's actual illumination distribution.

5. Conclusions

The TIM components have been calibrated using measurements at LASP and NIST as well as modelling. Ground calibrations include measurements of aperture areas, cavity reflectances, shutter waveforms and standard voltages and resistors. Noise measurements of the flight-ready instrument show $<2 \times 10^{-6}$ precision. On-orbit calibrations and corrections are made for system gain, thermal dark signal, sensitivity degradation and equivalence. Thorough system analysis and careful tracking of component uncertainties provide the expectation that the TIM will acquire TSI measurements with 10^{-4} relative standard uncertainty.

References

[1] Lawrence G M, Rottman G, Harder J and Woods T 2000 *Metrologia* **37** 407–10
[2] Lawrence G M, Rottman G, Kopp G, Harder J, McClintock W and Woods T 2000 *Proc. SPIE* (*Earth Observing Systems V*) **4135** 215–24
[3] Gundlach J H, Adelberger E G, Heckel B R and Swanson H E 1996 *Phys. Rev.* D **54** R1256–9
[4] Rice J P, Lorentz S R and Jung T M 1999 The next generation of active cavity radiometers for space-based remote sensing *Preprint Volume of the 10th Conf. Atmospheric Radiation (28 June–2 July 1999)* pp 85–8
[5] Steinmetz C P 1893 *Trans. AIEE* **10** 227–31
[6] Lathi B P 1998 *Signal Processing and Linear Systems* (Berkeley: Cambridge University Press)
[7] Fowler J, Saunders R and Parr A 1998 *Metrologia* **35** 497–500
[8] Shirley E 1998 *Appl. Opt.* **37** 6581–90
[9] Shirley E 2000 *NIST Report of Modeling 0000207602* p 32
[10] Lean J 2000 *Geophys. Res. Lett.* **27** 2425–8
[11] Hanssen, Leonard, NIST Optical Technology Division 2002 Private communication
[12] Spreadbury P J 1991 *IEEE Trans. Instrum. Meas.* **40** 343–6
[13] Press W, Teutolsky S, Vetterling W and Flannery B 1993 *Numerical Recipes: The Art of Scientific Computing* (Cambridge: Cambridge University Press)